

Cite this: *J. Mater. Chem. C*, 2021,  
9, 1221

# Constructing host- $\sigma$ -guest structures to optimize the efficiency of non-doped solution-processed OLEDs†

Dan Liu,<sup>‡a</sup> Meng Zhang,<sup>‡a</sup> Haowen Chen,<sup>a</sup> Daiyu Ma,<sup>a</sup> Wenwen Tian,<sup>a</sup>  
Kaiyong Sun,<sup>ab</sup> Wei Jiang<sup>id</sup>\*<sup>a</sup> and Yueming Sun\*<sup>a</sup>

Two novel host- $\sigma$ -guest emitters based on a blue emissive thermally activated delayed fluorescence (TADF) unit were designed and synthesized. By grafting 4TCzBN onto common host materials, these neat films (4TCzBN-*o*-PhCz and 4TCzBN-*o*-mCP) emit strong fluorescence with 39.4% and 60.8% photoluminescence quantum yields (PLQYs), respectively. And the oxygen-bridge linked host can not only suppress the triplet exciton quenching between guest units, but also improve the carrier transport ability. Non-doped OLEDs based on emitters formed by a solution process exhibit a maximum external quantum efficiency (EQE) of 8.0%, 24.9 cd A<sup>-1</sup> current efficiency (CE) and low efficiency roll off. These results indicate that the device performance can be improved by constructing a host- $\sigma$ -guest structure with the introduction of an *o*-bridge linked bipolar host. The strategy proposed in this paper may provide inspiration for the design of more efficient blue solution-processable TADF emitters.

Received 19th October 2020,  
Accepted 7th December 2020

DOI: 10.1039/d0tc04959j

rsc.li/materials-c

## Introduction

The development of high-performance non-doped organic light-emitting diodes (OLEDs) has been a great challenge in the research of OLEDs because most luminescent materials are unable to function efficiently in non-doped OLEDs because of severe concentration quenching and exciton annihilation.<sup>1–5</sup> For example, the conventional fluorescent and phosphorescent materials almost exhibit the aggregation-caused quenching (ACQ) phenomenon due to  $\pi$ - $\pi^*$  interactions of conjugated aromatic molecules or collision annihilation of long-lived triplet excitons of phosphors.<sup>6</sup> TADF molecules are no exception, and they also inevitably undergo triplet-triplet annihilation (TTA) and singlet-triplet annihilation (STA) owing to the low reverse intersystem crossing (RISC) rate.<sup>7</sup> So the emitters generally have to be dispersed into host matrices to alleviate concentration quenching.<sup>8</sup> Correspondingly, this doping process also derives other problems such as phase separation and complex preparation process.<sup>9</sup> Furthermore, it is very difficult to accurately control

the doping concentration when mixing two materials by vacuum deposition.<sup>10–12</sup> Therefore, there is a great demand to find new strategies to design high efficient non-doped emitters with strong emission.

To achieve such a goal, the molecular structure should be rationally designed. First of all, to achieve theoretically 100% exciton utilization, that is, to design thermally activated delayed fluorescent molecules with a small  $\Delta E_{ST}$  value, it is necessary to design DA-type molecules with twisted structures to reduce the overlap of the electron cloud of HOMO and LUMO.<sup>13–16</sup> The molecular design strategies related to small  $\Delta E_{ST}$  values have been reported and summarized by many researchers.<sup>17–19</sup> The repetitious details will not be given here. Secondly, as the light-emitting layer material in OLED devices, these emitters should fluoresce strongly in the thin film state with high PLQYs. To achieve this, the first thing that naturally comes to mind is the aggregation-induced emission (AIE) concept proposed by Tang *et al.*<sup>20–22</sup> Correspondingly, they also proposed many methods to enhance the luminescence in the solid state, such as limiting the vibration and rotation of molecules in the aggregate state.<sup>6,23–27</sup> Combining the above two aspects, what we have to do is to design high-performance luminescent materials with TADF and AIE properties.<sup>28,29</sup> However, most TADF molecules, like traditional fluorescent phosphorescent materials, inevitably undergo an aggregation quenching process through the TTA or STA pathway.<sup>41</sup> According to some literature reports, the fluorescence quenching in the TADF molecular system mainly occurs in triplet excitons, and its lifetime is in the ms range. These triplet

<sup>a</sup> Jiangsu Province Hi-Tech Key Laboratory for Bio-Medical Research, Jiangsu Engineering Laboratory of Smart Carbon-Rich Materials and Device, School of Chemistry and Chemical Engineering, Southeast University, Nanjing, 211189, China. E-mail: jiangw@seu.edu.cn, sun@seu.edu.cn

<sup>b</sup> School of Chemistry and Chemical Engineering, Yancheng Institute of Technology, Yancheng, Jiangsu 224051, China

† Electronic supplementary information (ESI) available. See DOI: 10.1039/d0tc04959j

‡ Dan Liu and Meng Zhang contributed equally to this work.

excitons undergo energy transfer through Dexter energy transfer (DET).<sup>7</sup> It is an intermolecular electron-exchange interaction, and the interaction distance is about 10–15 Å.<sup>8,30</sup> Therefore, the short-range nature of DET prompts us to make appropriate molecular modifications to inhibit the DET quenching process.

Based on the above ideas, we propose a new strategy to design novel solution processable TADF molecules 4TCzBN-*o*-PhCz and 4TCzBN-*o*-mCP, which using *o*-bridges to connect fluorescent guest fragments with host fragments. From the design perspective, we believe that the introduced host unit and peripheral *t*-butyl group will increase the intermolecular distance, further to suppress the collision quenching of triplet excitons.<sup>40</sup> Moreover, the host- $\sigma$ -guest co-system not only avoids the phase separation phenomenon that can easily occur in physical doping, but also improves the film-forming properties and the stability. At the same time, the energy transfer from the intramolecular host to the guest will also limit the exciton quenching between the guest units, which is also confirmed by the experimental results. 4TCzBN-*o*-mCP shows excellent blue emission with the TADF phenomenon and higher PLQY. The non-doped solution-processed OLEDs based on 4TCzBN-*o*-mCP demonstrate improved device performance with 24.9 cd A<sup>-1</sup> current efficiency (CE), 8.0% maximum external quantum efficiency (EQE), and 19.5 lm W<sup>-1</sup> luminance efficiency (LE). Obviously, they are more prominent than devices based on traditional TADF small molecule 4TCzBN. These results prove the feasibility of host- $\sigma$ -guest molecules and shed light on the development of new TADF molecules for efficient non-doped solution processed OLEDs.

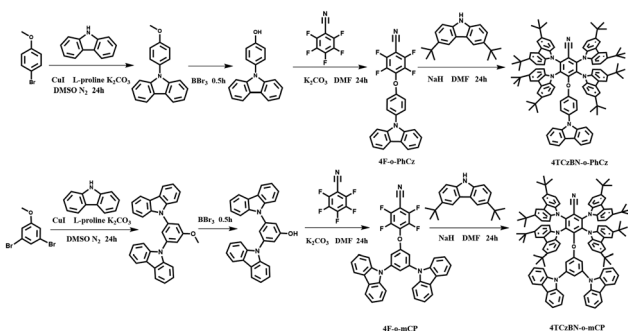
## Results and discussion

### 1. Materials and synthesis

Detailed synthesis of 4TCzBN-*o*-PhCz and 4TCzBN-*o*-mCP is demonstrated in the ESI.† As shown in Scheme 1, 4TCzBN-*o*-PhCz and 4TCzBN-*o*-mCP were synthesized *via* the nucleophilic reaction between the 4TCzBN and PhCz (mCP) derivative moieties. The chemical structures were confirmed by nuclear magnetic resonance (NMR) and mass spectroscopy.

### 2. Theoretical calculations

Theoretical calculations were first carried out to simulate the molecular structures and electronic transition properties.



Scheme 1 Synthetic routes of 4TCzBN-*o*-PhCz and 4TCzBN-*o*-mCP.

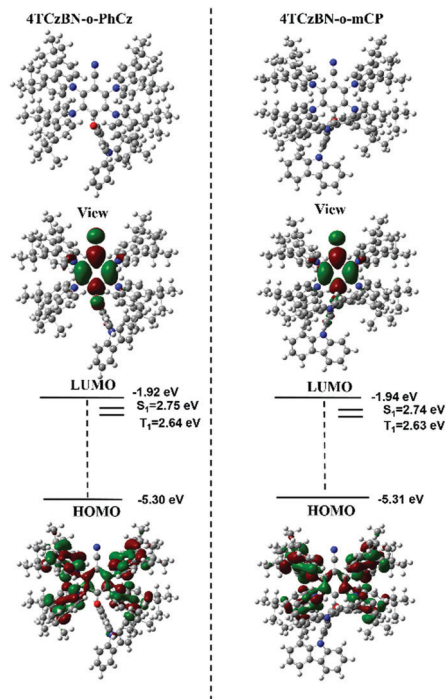


Fig. 1 Optimized geometries and electron cloud distribution maps of 4TCzBN-*o*-PhCz and 4TCzBN-*o*-mCP.

As shown in Fig. 1, 4TCzBN-*o*-PhCz and 4TCzBN-*o*-mCP have separated distribution of frontier orbitals. The highest occupied molecular orbitals (HOMOs) are predominantly centered on *tert*-butyl carbazole, while the lowest unoccupied molecular orbitals (LUMOs) are located on cyanobenzene. The  $\sigma$ -bonded phenylcarbazole (PhCz) and 3,5-diphenylcarbazole (mCP) units hardly contribute to the HOMO and LUMO, which indicates that *o*-bridge linked host fragments do not change the emission wavelength of the guest unit, but play a role in promoting the electron and hole transport. Similar spatial distributions of HOMOs and LUMOs are also observed for 4TCzBN.<sup>8</sup> The HOMO and LUMO of these compounds are spatially well separated and small  $\Delta E_{ST}$  can be anticipated. The calculated HOMO, LUMO,  $S_1$  and  $T_1$  values are listed in Table S1 (ESI†). According to Table S1 (ESI†), the *o*-bridge PhCz and mCP units can slightly reduce the values of  $\Delta E_{ST}$ , which are beneficial to achieve efficient thermally activated delayed fluorescence.<sup>31</sup>

### 3. Photophysical properties

The UV-Vis absorption and photoluminescence (PL) spectra of both new TADF emitters were investigated at room temperature. In toluene, both 4TCzBN-*o*-PhCz and 4TCzBN-*o*-mCP showed absorption peaks at around  $\sim$ 340 nm and  $\sim$ 410 nm. The strong absorption peaks at  $\sim$ 340 nm are ascribed to the  $\pi$ - $\pi^*$  transition. The relatively low-energy absorption peaks at 400–420 nm are derived from the charge-transfer (CT) transition from carbazole to cyanobenzene. The energy gaps ( $E_g$ ) were calculated using maximum absorption edges and the values matched well with the simulation results. The maximum PL peak of 4TCzBN-*o*-PhCz and 4TCzBN-*o*-mCP in 10<sup>-5</sup> M toluene

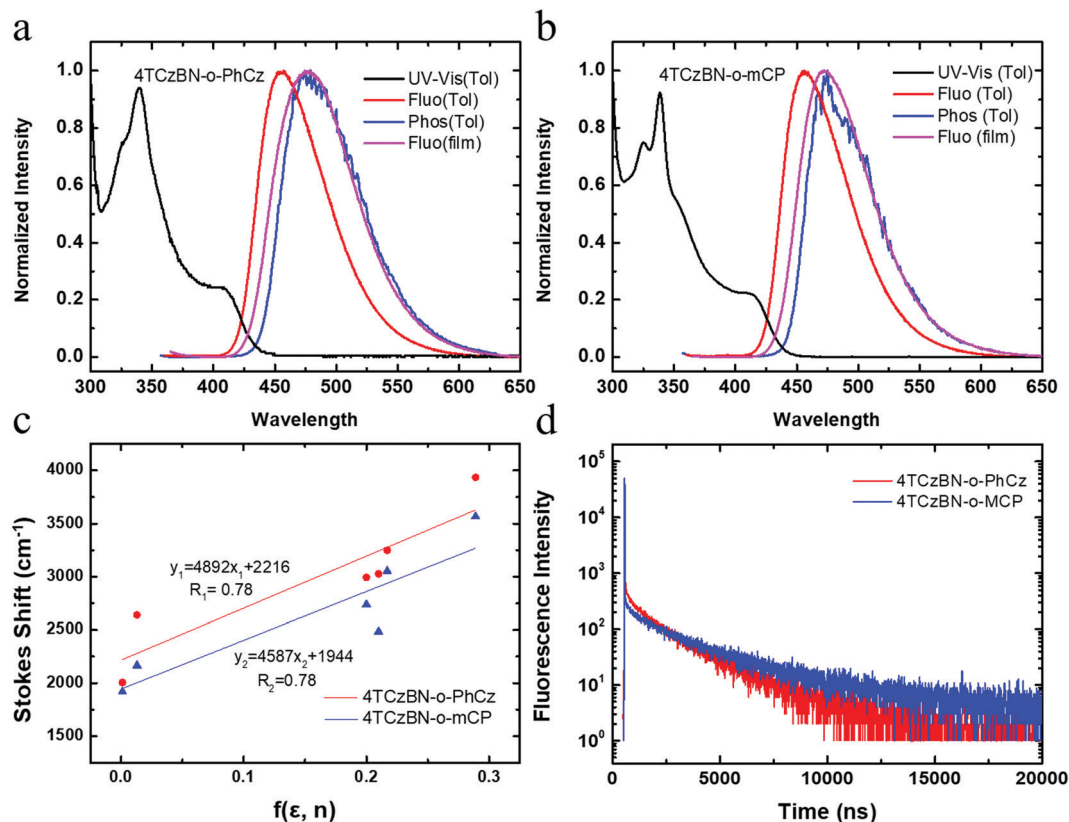


Fig. 2 The UV-Vis, fluorescence and phosphorescence spectra of 4TCzBN-*o*-PhCz (a) and 4TCzBN-*o*-mCP (b), where the Phos spectra were recorded in toluene at 77 K with 10 ms delayed time. (c) Plots of Stokes shift versus orientation polarization ( $\Delta f$ ) of the solvent. (d) Transient PL decay spectra in neat films measured at room temperature for 4TCzBN-*o*-PhCz and 4TCzBN-*o*-mCP.

was observed at 456 nm, which is the same as that of 4TCzBN. Fig. 2 and Fig. S1 (ESI<sup>†</sup>) also show the Phos spectra in a frozen toluene matrix at 77 K. The phosphorescence (Phos) spectra of 4TCzBN, 4TCzBN-*o*-PhCz and 4TCzBN-*o*-mCP are well resolved and show characteristic vibrational structures, and the peaks are at 473 nm, 477 nm, and 473 nm, respectively. The values of the  $S_1$  and  $T_1$  energy levels of these compounds measured from the onset of the steady PL/Phos spectra are all 2.90/2.80 eV, 2.94/2.83 eV, and 2.90/2.82 eV, respectively.<sup>32</sup> Thus, the experimental  $\Delta E_{ST}$  values are 0.10 eV, 0.11 eV and 0.08 eV for 4TCzBN, 4TCzBN-*o*-PhCz and 4TCzBN-*o*-mCP, respectively (Table 1). The smaller  $\Delta E_{ST}$  value of 4TCzBN-*o*-mCP can lead to fast spin-flip and efficient RISC due to the stronger steric hindrance introduced by mCP. The emission and PLQY of their neat films also support the opinion; the maximum wavelengths are 471 nm,

474 nm and 471 nm for 4TCzBN, 4TCzBN-*o*-PhCz and 4TCzBN-*o*-mCP. 4TCzBN-*o*-mCP showed the same emission wavelength as 4TCzBN even if a polar host matrix was introduced. It is mainly because the sterically shielded fragments decrease the intermolecular interaction and  $\pi$ - $\pi$  stacking.<sup>33</sup> The red-shifted emission and increased  $\Delta E_{ST}$  value of 4TCzBN-*o*-PhCz can be interpreted as the rotation and the polarity of the introduced PhCz unit, and it was further confirmed by the solvatochromic effect measurements.

Furthermore, to confirm the better structural stability in the host- $\sigma$ -guest structure, we recorded the absorption and emission spectra in solvents with different polarities. As can be seen from Fig. S1 and S2 (ESI<sup>†</sup>), no significant solvent polarity dependent spectral shifts in the absorption spectra were observed for these emitters. This indicates that, in their ground states, these

Table 1 Basic photophysical and electrochemical parameters of 4TCzBN, 4TCzBN-*o*-PhCz and 4TCzBN-*o*-mCP

Materials	$T_d, T_g$	$\lambda_{abs}^a$ [nm]	$\lambda_{em}^{bcde}$ [nm]	$E_g^f$ [eV]	$S_1/T_1^{gh}$ [eV]	$\Delta E_{ST}^i$ [eV]	HOMO <sup>j</sup> [eV]	LUMO <sup>k</sup> [eV]
4TCzBN	448, —	341, 416	456, 472, 486, 471	2.80	2.90/2.80	0.10	-5.24	-2.44
4TCzBN- <i>o</i> -PhCz	421, —	339, 409	456, 473, 486, 474	2.84	2.94/2.83	0.11	-5.20	-2.36
4TCzBN- <i>o</i> -mCP	462, 223	338, 414	456, 470, 483, 471	2.81	2.90/2.82	0.08	-5.21	-2.40

<sup>a</sup> Measured in toluene solution at 300 K. <sup>b</sup> Measured in toluene solution. <sup>c</sup> Measured in  $CH_2Cl_2$  solution. <sup>d</sup> Measured in ethanol solution. <sup>e</sup> Measured in films at 300 K. <sup>f</sup> Estimated from the absorption edges in toluene. <sup>g</sup> Calculated from the onset of the fluorescence spectra in toluene at 300 K. <sup>h</sup> Estimated from the onset of the phosphorescence spectra in toluene at 77 K. <sup>i</sup> The difference between  $S_1$  energy and  $T_1$  energy. <sup>j</sup> Determined by the onset of the oxidation curves.  $E_{HOMO} = E_{ref} - E_{ox}$ . <sup>k</sup> Calculated from the energy gap and HOMO.

chromophores are not significantly stabilized by solvation due to a relatively small dipole moment. Conversely, as shown in Fig. S1 and S2 (ESI<sup>†</sup>), strong solvatochromic red-shifts of the emission spectra were observed for compounds 4TCzBN, 4TCzBN-*o*-PhCz and 4TCzBN-*o*-mCP with increasing solvent polarity. This demonstrates that the emission originates from the charge transfer (CT) states. Therefore, the maximum red shifts observed in the emission spectra when increasing the polarity were 44 nm, 44 nm and 40 nm for 4TCzBN, 4TCzBN-*o*-PhCz and 4TCzBN-*o*-mCP, respectively. The Stokes shift ( $\nu_a - \nu_f$ ) can be calculated using the biggest absorption peaks and the emission peaks of the compounds, as summarized in Table S2 (ESI<sup>†</sup>). According to the plots of ( $\nu_a - \nu_f$ ) vs.  $\Delta f$ , all emitters obey a linear relationship with notable positive slopes (Fig. 2c).<sup>34</sup> Compared to 4TCzBN and 4TCzBN-*o*-PhCz (Fig. S1, ESI<sup>†</sup>), the slopes of 4TCzBN-*o*-mCP is even smaller; these observations clearly indicated that these compounds exhibited smaller dipole moment change ( $\Delta\mu$ ) between the ground states and the excited states. And then the dipole moments of the three compounds were calculated using the Lippert–Mataga equation, and 4TCzBN-*o*-mCP shows the smallest change in dipole moment, followed by 4TCzBN, and 4TCzBN-*o*-PhCz shows the largest change, which is consistent with the simulation calculated data. It is because the introduced large steric hindrance unit mCP can stabilize the excited state configuration to a certain extent.

In order to research the photophysical variation trend of these compounds from the dispersed state to the aggregated state, we studied the emission spectra of 4TCzBN, 4TCzBN-*o*-PhCz and 4TCzBN-*o*-mCP under mixing volume ratios of solutions containing water and tetrahydrofuran (THF); the fluorescence intensities of these compounds showed interesting change (Fig. 3). The PL intensity gradually decreased as the volume fractions of water ( $f_w$ ) increased until  $f_w = 50\%$  (4TCzBN) or 60% (4TCzBN-*o*-PhCz and 4TCzBN-*o*-mCP). Subsequently, the PL intensity sharply increased with the formation of nanoparticles owing to the continuing increased water ratios. The trend can be interpreted by the twist intramolecular charge transfer (TICT) effect.<sup>35,36</sup> Before the generation of aggregates, solvatochromism accounts for the red-shift of the emission peak with increasing solvent polarity. In contrast, after the generation of nano-aggregates, the intramolecular rotation is restricted and the local environment becomes less polar, thereby resulting in a blueshift in the emission color. It is worth mentioning that the maximum-wavelength variation of 4TCzBN-*o*-mCP in different water fractions is not obvious. It also indicated that introducing the mCP host unit can stabilize the molecular configuration in excited states and this twist molecular structure can suppress the  $\pi$ - $\pi^*$  stacking further to inhibit concentration quenching.

The transient PL characteristics of these emitters were measured. As can be seen from Fig. 2d, prompt and delayed components were clearly observed from the transient PL decay

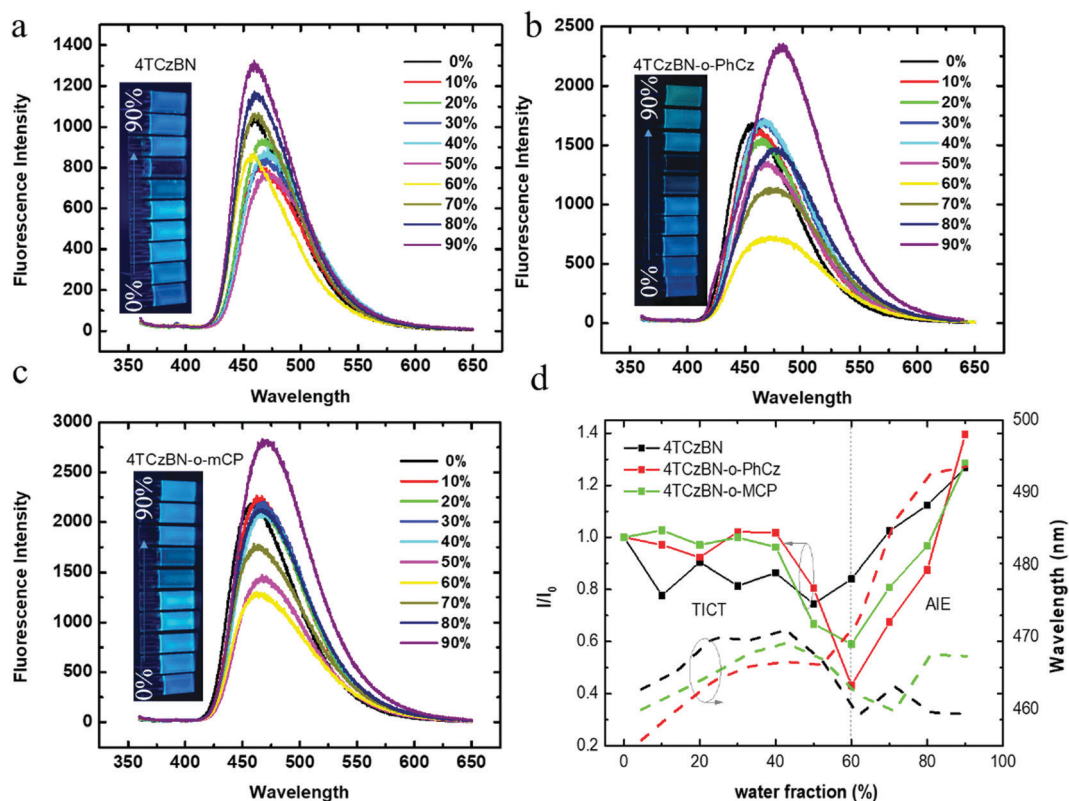


Fig. 3 PL spectra and emission images of 4TCzBN (a), 4TCzBN-*o*-PhCz (b) and 4TCzBN-*o*-mCP (c) in THF–water mixtures ( $10^{-5}$  M) with different fractions of water, respectively, under 365 nm UV irradiation. (d) The plots of the fluorescence ratio ( $I/I_0$ ) and peak wavelength versus the water volume fraction, where  $I_0$  is the initial fluorescence intensity.

curves of both emitters. The behaviors confirmed that these compounds were TADF materials. The PLQY also was measured to evaluate the superiority of the molecular design. 4TCzBN-*o*-mCP has a higher PLQY with 60.8% than 4TCzBN-*o*-PhCz (39.4%) in the neat film state. The fluo decay rate ( $k_F$ ) and the rate of RISC ( $k_{RISC}$ ) were also calculated and are summarized in Table S3 (ESI<sup>†</sup>). The introduction of mCP units induces lower  $k_{nr}$ , and higher  $k_{RISC}$  and  $\phi_{RISC}$ . Therefore, the introduction of the mCP host increases the luminescence intensity owing to smaller  $\Delta E_{ST}$  and suppressed non-radiative deactivation.

#### 4. The electrochemical and thermal properties

The practical energy levels of the luminogens are evaluated by cyclic voltammetry (CV) measurements. As can be seen from Fig. S3 (ESI<sup>†</sup>), all the compounds show similar oxidation processes. The HOMO energy levels of 4TCzBN, 4TCzBN-*o*-PhCz and 4TCzBN-*o*-mCP are estimated to be  $-5.24$ ,  $-5.20$  and  $-5.21$  eV, respectively. The shallower HOMO levels in the host- $\sigma$ -guest structure are attributed to the stronger donor ability owing to the introduction of *o*-bridge host units PhCz and mCP. The LUMO values were calculated as  $-2.44$ ,  $-2.36$  and  $-2.40$  eV for 4TCzBN, 4TCzBN-*o*-PhCz and 4TCzBN-*o*-mCP by the equation  $E_{LUMO} = E_{HOMO} + E_g$ , where the energy gap ( $E_g$ ) is obtained using the absorption edges. Overall speaking, the HOMO and LUMO levels of these compounds are similar and the introduction of host fragments hardly affects the energy level of the guest emitters. This is in line with the original intention of molecular design. Furthermore, the thermal

stability of these emitters was investigated (Fig. S3, ESI<sup>†</sup>) and these compounds show good thermal stability with decomposition temperatures in the range of  $421$ – $462$  °C and a high glass transition temperature ( $T_g$ ) in the range of  $223$ – $322$  °C, in which the  $T_g$  of 4TCzBN is reported at  $322$  °C.<sup>8</sup> Such excellent thermal properties readily endow OLEDs based on them with high morphological stability, favorable for the OLED stability during operation. Moreover, the AFM picture of these neat films is shown in Fig. S4 (ESI<sup>†</sup>), and the small root mean square (RMS) roughness show good film-forming properties and no phase separation, which are beneficial to fabricate non-doped solution-processed OLEDs.<sup>37–39</sup> It also indicated that the solubilized *tert*-butyl and nonconjugated oxygen bridges can improve the morphological stability of neat films.

#### 5. The electroluminescence properties

Inspired by the high thermal stability and good film forming ability of the host- $\sigma$ -guest structure, simple double-layer non-doped solution-processed OLEDs were fabricated with an architecture of ITO/PEDOT:PSS (40 nm)/4TCzBN (Device A), 4TCzBN-*o*-PhCz (Device B) or 4TCzBN-*o*-mCP (Device C) (50 nm)/PO-T2T (40 nm)/Cs<sub>2</sub>CO<sub>3</sub> (2 nm)/Al (Fig. 4a), where poly(3,4-ethylenedioxythiophene) doped with poly-(styrenesulfonate) (PEDOT:PSS) served as a hole-injecting layer and 2,4,6-tris[3-(diphenylphosphinyl)phenyl]-1,3,5-triazine (PO-T2T) acted as an electron transporting layer (ETL). Fig. 4 shows the current density–voltage–luminance ( $J$ – $V$ – $L$ ) characteristics, the EL spectra, and the EQEs *versus* luminance curves of Devices A–C. The

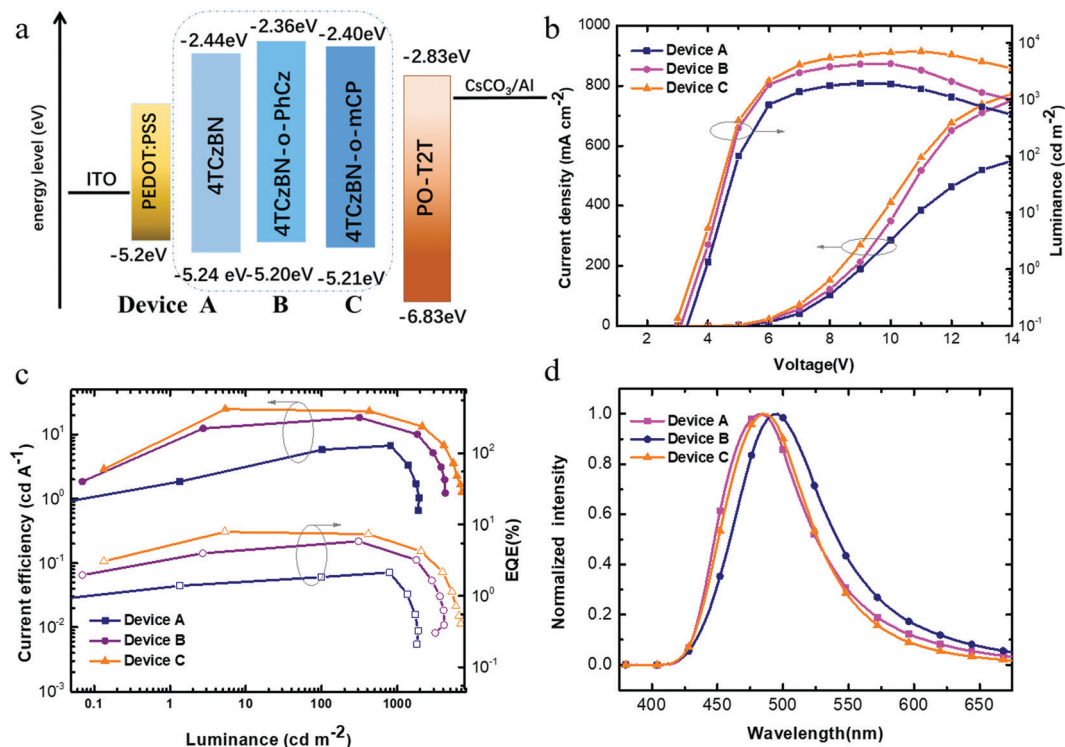


Fig. 4 (a) Energy-level arrangement of the organic materials used in the OLED devices; (b) current density–voltage–luminance ( $J$ – $V$ – $L$ ) characteristics of devices A–C; (c) current efficiencies *versus* brightness and the external quantum efficiency *versus* brightness; and (d) electroluminescence spectra of devices A–C.

**Table 2** Electroluminescent performances of non-doped solution-processed OLEDs based on 4TCzBN, 4TCzBN-*o*-PhCz and 4TCzBN-*o*-mCP emitters

Device	Emitter	$V_{\text{on}}^a$	EL (nm)	$\text{CE}_{\text{max}}^b$	$\text{PE}_{\text{max}}^c$	$\text{EQE}_{\text{max}}^d$	$\text{CE}^e$	$L_{\text{max}}^f$	CIE (x,y) <sup>g</sup>
A	4TCzBN	3.9	484	6.7	4.7	2.1	6.1/5.0	2000	(0.19,0.30)
B	4TCzBN- <i>o</i> -PhCz	3.7	496	18.4	11.6	5.9	16.7/12.1	4300	(0.22,0.39)
C	4TCzBN- <i>o</i> -mCP	3.5	484	24.9	19.5	8.0	24.2/14.3	7000	(0.18,0.31)

<sup>a</sup>  $V_{\text{on}}$  = turn-on voltage at 1 cd m<sup>-2</sup>. <sup>b</sup>  $\text{CE}_{\text{max}}$  = maximum current efficiency. <sup>c</sup>  $\text{PE}_{\text{max}}$  = maximum power efficiency. <sup>d</sup>  $\text{EQE}_{\text{max}}$  = maximum external quantum efficiency. <sup>e</sup> Current efficiency at luminances of 100 cd m<sup>-2</sup> and 1000 cd m<sup>-2</sup>. <sup>f</sup>  $L_{\text{max}}$  = maximum luminance. <sup>g</sup> CIE = the Commission Internationale de L'Eclairage coordinates.

characteristic data for all devices are summarized in Table 2. The turn-on voltages of Devices B (3.7 V) and C (3.5 V) are significantly lower than the corresponding Device A (3.9 V). The superior electroluminescent performance of 4TCzBN-*o*-mCP is attributed to the better matched HOMO and LUMO energy levels that reduce the hole and electron injection barriers of Device C. Device C exhibits considerably high luminance and current density at the same bias. A maximum current efficiency ( $\eta_{\text{c,max}}$ ) of 24.9 cd A<sup>-1</sup>, a maximum power efficiency ( $\eta_{\text{p,max}}$ ) of 19.5 lm W<sup>-1</sup>, and a maximum external quantum efficiency ( $\eta_{\text{ext,max}}$ ) of 8.0% were achieved. It is worth mentioning that these devices exhibit very high color stability at the elevated operating temperatures which is one of the prerequisites for practical application. Moreover, these devices show rather low efficiency roll-off values than that based on 4TCzBN. The non-doped devices show blue emission with emission peaks at 484 nm, 496 nm, and 484 nm for 4TCzBN, 4TCzBN-*o*-PhCz and 4TCzBN-*o*-mCP, respectively. This is mainly because the introduction of PhCz fragments increased the intramolecular movement. It has been confirmed by the solvation effect measurement and theoretical simulation. The results with the same emission but higher device efficiency of 4TCzBN-*o*-mCP further illustrates that the introduction of the host can suppress the collision quenching between excitons. Therefore, it is believed that the molecular design can optimize non-doped solution-processed OLEDs.

## Conclusions

In summary, a novel molecular design of grafting an TADF unit, 2,3,5,6-tetrakis(3,6-di-*tert*-butyl-9H-carbazol-9-yl)benzotrile (4TCzBN) to common host materials (PhCz and mCP) is proposed and realized. The photophysical properties, electronic structures and electrochemical behaviors of the generated luminogens are similar to those of 4TCzBN, demonstrating that the host fragments do not affect the emission of the guest. However, in the neat film state, the host- $\sigma$ -guest materials turn out to be superior emitters with conspicuous delay fluorescence and higher PLQY. The steric shielded host units can increase the distance of guest fragments, further inhibiting the triplet exciton quenching by depressing Dexter energy transfer. Owing to higher exciton utilization and bipolar carrier transport ability, the nondoped solution-processed blue OLEDs based on 4TCzBN-*o*-mCP show excellent device performance, with a maximum luminance of 7000 cd m<sup>-2</sup>, an EQE of 8.0% and 19.5 lm W<sup>-1</sup> power efficiency. The results strongly proved the

feasibility and versatility of the proposed molecular design, and it will be of high significance for the advancement of solution-processed OLEDs.

## Conflicts of interest

There are no conflicts to declare.

## Acknowledgements

We are grateful for the grants from the National Natural Science Foundation of China (21875036 and 21801216), the Fundamental Research Funds for the Central Universities (2242019K40150). We are also thankful for the support from the Scientific Research Foundation of Graduate School of Southeast University (YBPY1975), the Priority Academic Program Development of Jiangsu Higher Education Institutions, and Nanjing Science and Technology Committee.

## References

- H. Liu, J. Zeng, J. Guo, H. Nie, Z. Zhao and B. Z. Tang, *Angew. Chem., Int. Ed.*, 2018, **57**, 9290–9294.
- X. L. Chen, J. H. Jia, R. Yu, J. Z. Liao, M. X. Yang and C. Z. Lu, *Angew. Chem., Int. Ed.*, 2017, **56**, 15006–15009.
- Y. Li, G. Xie, S. Gong, K. Wu and C. Yang, *Chem. Sci.*, 2016, **7**, 5441–5447.
- M. Godumala, S. Choi, M. J. Cho and D. H. Choi, *J. Mater. Chem. C*, 2019, **7**, 2172–2198.
- X. Ban, W. Jiang, T. Lu, X. Jing, Q. Tang, S. Huang, K. Sun, B. Huang, B. Lin and Y. Sun, *J. Mater. Chem. C*, 2016, **4**, 8810–8816.
- Y. Li, S. Liu, H. Ni, H. Zhang, H. Zhang, C. Chuah, C. Ma, K. S. Wong, J. W. Y. Lam, R. T. K. Kwok, J. Qian, X. Lu and B. Z. Tang, *Angew. Chem., Int. Ed.*, 2020, **59**, 12822–12826.
- J. Huang, H. Nie, J. Zeng, Z. Zhuang, S. Gan, Y. Cai, J. Guo, S. J. Su, Z. Zhao and B. Z. Tang, *Angew. Chem., Int. Ed.*, 2017, **56**, 12971–12976.
- D. Zhang, M. Cai, Y. Zhang, D. Zhang and L. Duan, *Mater. Horiz.*, 2016, **3**, 145–151.
- J. Li, R. Zhang, Z. Wang, B. Zhao, J. Xie, F. Zhang, H. Wang and K. Guo, *Adv. Opt. Mater.*, 2018, **6**, 1701256.
- X. Lv, W. Zhang, D. Ding, C. Han, Z. Huang, S. Xiang, Q. Zhang, H. Xu and L. Wang, *Adv. Opt. Mater.*, 2018, **6**, 1800165.

- 11 Y. Miao, K. Wang, L. Gao, B. Zhao, H. Wang, F. Zhu, B. Xu and D. Ma, *J. Mater. Chem. C*, 2018, **6**, 8122–8134.
- 12 Z. Wu, L. Yu, F. Zhao, X. Qiao, J. Chen, F. Ni, C. Yang, T. Ahamad, S. M. Alshehri and D. Ma, *Adv. Opt. Mater.*, 2017, **5**, 1700415.
- 13 K. Goushi, K. Yoshida, K. Sato and C. Adachi, *Nat. Photonics*, 2012, **6**, 253–258.
- 14 H. Uoyama, K. Goushi, K. Shizu, H. Nomura and C. Adachi, *Nature*, 2012, **492**, 234–238.
- 15 Z. Yang, Z. Mao, Z. Xie, Y. Zhang, S. Liu, J. Zhao, J. Xu, Z. Chi and M. P. Aldred, *Chem. Soc. Rev.*, 2017, **46**, 915–1016.
- 16 Y. Im, M. Kim, Y. J. Cho, J.-A. Seo, K. S. Yook and J. Y. Lee, *Chem. Mater.*, 2017, **29**, 1946–1963.
- 17 Q. Wei, N. Fei, A. Islam, T. Lei, L. Hong, R. Peng, X. Fan, L. Chen, P. Gao and Z. Ge, *Adv. Opt. Mater.*, 2018, **6**, 1800512.
- 18 Y. Zou, S. Gong, G. Xie and C. Yang, *Adv. Opt. Mater.*, 2018, 1800568.
- 19 J. H. Kim, J. H. Yun and J. Y. Lee, *Adv. Opt. Mater.*, 2018, **6**, 1800255.
- 20 Z. Zhao, H. Zhang, J. W. Y. Lam and Z. Tang Ben, *Angew. Chem., Int. Ed.*, 2020, **59**, 9888–9907.
- 21 H. Zhang, Z. Zhao, A. T. Turley, L. Wang, P. R. McGonigal, Y. Tu, Y. Li, Z. Wang, R. T. K. Kwok, J. W. Y. Lam and B. Z. Tang, *Adv. Mater.*, 2020, 202001457.
- 22 B. Liu and B. Z. Tang, *Angew. Chem., Int. Ed.*, 2020, **59**, 9788–9789.
- 23 W. Z. Yuan, P. Lu, S. Chen, J. W. Y. Lam, Z. Wang, Y. Liu, H. S. Kwok, Y. Ma and B. Z. Tang, *Adv. Mater.*, 2010, **22**, 2159–2163.
- 24 R. Hu, J. W. Y. Lam, Y. Liu, X. Zhang and B. Z. Tang, *Chem. – Eur. J.*, 2013, **19**, 5617–5624.
- 25 N. L. C. Leung, N. Xie, W. Yuan, Y. Liu, Q. Wu, Q. Peng, Q. Miao, J. W. Y. Lam and B. Z. Tang, *Chem. – Eur. J.*, 2014, **20**, 15349–15353.
- 26 J. Li, Y. Zhang, J. Mei, J. W. Y. Lam, J. Hao and B. Z. Tang, *Chem. – Eur. J.*, 2015, **21**, 907–914.
- 27 Z. Zhao, X. Zheng, L. Du, Y. Xiong, W. He, X. Gao, C. Li, Y. Liu, B. Xu, J. Zhang, F. Song, Y. Yu, X. Zhao, Y. Cai, X. He, R. T. K. Kwok, J. W. Y. Lam, X. Huang, D. L. Phillips, H. Wang and B. Z. Tang, *Nat. Commun.*, 2019, **10**, 2952.
- 28 J. Guo, J. Fan, L. Lin, J. Zeng, H. Liu, C. K. Wang, Z. Zhao and B. Z. Tang, *Adv. Sci.*, 2019, **6**, 1801629.
- 29 J. Zeng, J. Guo, H. Liu, J. W. Y. Lam, Z. Zhao, S. Chen and B. Z. Tang, *Chem. – Asian J.*, 2019, **14**, 828–835.
- 30 D. Liu, K. Sun, G. Zhao, J. Wei, J. Duan, M. Xia, W. Jiang and Y. Sun, *J. Mater. Chem. C*, 2019, **7**, 11005–11013.
- 31 Q. Zhang, J. Li, K. Shizu, S. Huang, S. Hirata, H. Miyazaki and C. Adachi, *J. Am. Chem. Soc.*, 2012, **134**, 14706–14709.
- 32 T. Hosokai, H. Matsuzaki, H. Nakanotani, K. Tokumaru, T. Tsutsui, A. Furube, K. Nasu, H. Nomura, M. Yahiro and C. Adachi, *Sci. Adv.*, 2017, **3**, e1603282.
- 33 H. Liu, J. Guo, Z. Zhao and B. Z. Tang, *ChemPhotoChem*, 2019, **3**, 993–999.
- 34 H.-H. Lin, Y.-C. Chan, J.-W. Chen and C.-C. Chang, *J. Mater. Chem.*, 2011, **21**, 3170–3177.
- 35 W. Z. Yuan, Y. Gong, S. Chen, X. Y. Shen, J. W. Y. Lam, P. Lu, Y. Lu, Z. Wang, R. Hu, N. Xie, H. S. Kwok, Y. Zhang, J. Z. Sun and B. Z. Tang, *Chem. Mater.*, 2012, **24**, 1518–1528.
- 36 S. Liu, X. Zhou, H. Zhang, H. Ou, J. W. Y. Lam, Y. Liu, L. Shi, D. Ding and B. Z. Tang, *J. Am. Chem. Soc.*, 2019, **141**, 5359–5368.
- 37 D. Zhang, X. Song, A. J. Gillett, B. H. Drummond, S. T. E. Jones, G. Li, H. He, M. Cai, D. Credgington and L. Duan, *Adv. Mater.*, 2020, **32**, 1908355.
- 38 Y. Zhang, D. Zhang, J. Wei, X. Hong, Y. Lu, D. Hu, G. Li, Z. Liu, Y. Chen and L. Duan, *Angew. Chem., Int. Ed.*, 2020, **59**, 17499–17503.
- 39 C. Zhang, Y. Lu, Z. Liu, Y. Zhang, X. Wang, D. Zhang and L. Duan, *Adv. Mater.*, 2020, 2004040.
- 40 G. Xie and L. Ding, *Sci. Bull.*, 2020, **65**(21), 1780–1782.
- 41 R. Ieuji, K. Goushi and C. Adachi, *Nat. Commun.*, 2019, **10**, 5283.